SACLANTCEN REPORT
serial no.: SR-236

SACLANT UNDERSEA
RESEARCH CENTRE

REPORT

# Single mode excitation, attenuation and backscatter in shallow water

D.F. Gingras

October 1995

The SACLANT Undersea Research Centre provides the Supreme Allied Commander Atlantic (SACLANT) with scientific and technical assistance under the terms of its NATO charter, which entered into force on 1 February 1963. Without prejudice to this main task – and under the policy direction of SACLANT – the Centre also renders scientific and technical assistance to the individual NATO nations.

Page count for SR-236 (excluding Covers and Data Sheet)

| Pages | Total |
|---|---|
| i–vi | 6 |
| 1–27 | 27 |
| | 33 |

SACLANT Undersea Research Centre
Viale San Bartolomeo 400
19138 San Bartolomeo (SP), Italy

tel: +39-187-540.111
fax: +39-187-524.600

e-mail: library@saclantc.nato.int

NORTH ATLANTIC TREATY ORGANIZATION

SACLANTCEN SR-236

# Single mode excitation, attenuation and backscatter in shallow water

D.F. Gingras

---

The content of this document pertains to work performed under Project 02 of the SACLANTCEN Programme of Work. The document has been approved for release by The Director, SACLANTCEN.

David L. Bradley
Director

intentionally blank page

# Single mode excitation, attenuation and backscatter in shallow water

D.F. Gingras

**Executive Summary:** It is well known that in shallow water the ocean bottom exerts a strong influence on acoustic propagation. Two important effects of the bottom influence are attenuation due to bottom interaction and backscatter generated by reflections from the water/sediment interface. For the active sonar application both of these factors are important and affect the design of the active sonar system.

In this report the use of a vertical array of sources weighted so as to excite only one mode was considered. It was demonstrated, via simulation, that a vertical array of sources driven in an appropriate frequency band can be used to minimize the combined effects of attenuation and bottom-generated backscatter in shallow water. Several bottom types along with summer and winter sound-speed profiles were considered. The results indicate that an optimum frequency band providing both minimum attenuation and minimum bottom-generated backscatter exists, and that the optimum frequency band is dependent on the bottom type.

The results of this study indicate that a vertical source array should provide improvements for active signal detection in shallow water. An experimental system should be built and demonstrated in a variety of shallow-water areas.

intentionally blank page

# Single mode excitation, attenuation and backscatter in shallow water

D.F. Gingras

**Abstract:** Normal mode theory is used to illustrate that a vertical array of weighted sources driven in an appropriate frequency band can be used to minimize the combined effects of attenuation and bottom-generated backscatter in shallow water. Results are presented for three canonical geoacoustic models using both a winter and summer sound speed profile. It is shown that through selective excitation of only mode 1 there exists an optimum frequency band providing both minimum attenuation and minimum bottom-generated backscatter. The results indicate that the center frequency of the optimum band increases as the critical angle decreases.

**Keywords:** attenuation ○ bottom backscatter ○ geoacoustic models ○ selective excitation ○ shallow water

# Contents



**Acknowledgements:** The author is indebted to Mr Edward Hug, formerly of the Naval Underwater Systems Center, for reviving interest in selective mode excitation work. The author also wishes to acknowledge the contributions of Dr Michael Collins of the Naval Research Laboratory who provided the FEPE two-way code and valuable assistance on its use, and Mr Silvio Bongi of SACLANTCEN for his careful modifications of the FEPE two-way code.

# 1 Introduction

It has long been known that the ocean bottom can exert a strong influence on acoustic propagation in shallow water, see for example [1–5] and the references therein. Two important effects of the bottom influence are attenuation due to bottom interaction and backscatter generated by reflection from the water/sediment interface. For shallow-water applications it may be useful to consider spatial focusing of the signal energy away from the water/sediment interface in order to reduce the effects of bottom interaction and reflection. By exploiting the geometric and geoacoustic characteristics of the shallow-water channel it is possible to accomplish this focusing by proper design of the signal transmitter.

The objective of this report is to identify those aspects of a signal transmitter which minimize the effect of attenuation and scattering on signal propagation in shallow water. This can be accomplished through the exploitation of two well-known shallow-water phenomena. First, individual modes can be excited, and second, each mode has a frequency band of minimum attenuation. Using the fact that the first mode often experiences the least attenuation and propagates with the smallest grazing angle leads to a transmitter design that excites only the first mode. Excitation of only the first mode, in the frequency band of minimum attenuation, will provide an optimum shallow-water propagation situation. The determination of the frequency band that provides minimum attenuation and minimum bottom-generated backscatter was an important aspect of this analysis. Surface scattering effects were not considered in the analysis, but since mode 1 propagates with a small grazing angle the surface scattering effects due to surface interaction will also be reduced.

There has been a significant amount of work conducted on the use of a vertical array of receivers and/or sources to isolate individual modes in an underwater channel. Ingenito [6] showed that mode separation could be achieved experimentally in shallow water for both range-independent and range-dependent environments. King [7] reported on experimental results aimed towards individual mode enhancement. Gazanhes *et al.* [8] reported on successful experimental mode identification work in a reduced scale model waveguide. Clay and Huang [9] also reported on experimental work in a scale model waveguide where the first mode was excited by shading a vertical array in amplitude to match the mode 1 eigenfunction. Finally, Gazanhes and Garnier [10] reported on a comprehensive set of mode excitation and filtering experiments in a scale model waveguide where mode interference and mode conversion was also examined. As all of the previous work was directed towards the demonstration that individual modes could be excited or identified, the effect of single-mode excitation on the forward or backscattered field was not investigated.

The first evaluation of the effect of single-mode excitation on the backscattered field appeared in Ref. [11].

A commonly observed effect in shallow water is that the ocean bottom acts as a low-loss acoustic reflector confining the acoustic energy to a duct, bounded below by the ocean bottom and above by the pressure release surface. Such a waveguide has the property that each of the propagating modes has a low-frequency cutoff. High frequencies are attenuated both by seawater absorption and bottom interaction leaving a band capable of propagating acoustic signals with relatively low loss. The presence of an optimal propagation band for shallow water was investigated by Jensen and Kuperman by comparing theory with experimental results [12]. Later, Eller and Gershfeld investigated the optimum frequency of propagation issue analytically using canonical bottom models [13].

The approach followed herein employs a transmitter consisting of a vertical array of sources (with 12 and 24 sources) weighted in amplitude and polarity to excite only mode 1. The number of sources was selected to coincide with an experimental system currently under development. The optimum frequency issue was addressed by evaluating the mode 1 attenuation as a function of frequency to determine the frequency band of minimum attenuation. The bottom-generated backscatter was evaluated using a single source, a source array with 12 sources and a source array with 24 sources as a function of frequency over the range from 200 to 1000 Hz. The backscatter was evaluated using random realizations of bathymetry profiles generated using a linear stochastic model. Average backscatter was computed over multiple realizations of the random bathymetry profile. The two-way parabolic equation model developed by Collins and Evans was used for backscatter computations [14]. The analysis was carried out for three cases of geoacoustic parameters with a winter and summer sound speed profile in a shallow-water channel.

# 2 Background

A considerable amount of fundamental research on shallow-water propagation and scattering has been accomplished, much of this work can be applied to the analysis of signal transmission schemes that optimally exploit shallow-water channel characteristics. With the availability of highly accurate and efficient propagation codes and high-speed computing, simulations can be carried out to investigate the performance of transmitters using selective mode excitation in realistic shallow-water channels.

*A. Mode excitation and filtering* The introduction of a directional source into the calculation of the acoustic field using normal modes was first discussed by Bucker and Morris in 1965 [15]. In that paper the authors indicated that the introduction of directional sources into the normal-mode calculations was quite straightforward and provided a solution based on superposition. In 1966 Clay [16] provided the theoretical framework for understanding the use of vertical arrays as mode filters. In 1974 Williams and Novak [17] discussed the issue of using a vertical array of discrete sources to excite or receive a single mode and provided a directivity pattern for excitation of the first mode in shallow water. The only at-sea experimental results involving a vertical source array in shallow water were reported by King in 1974; he showed results obtained at a site in the Block Island Sound [7]. Through the use of amplitude and phase shading of the source array he successfully enhanced the signal level at desired locations in the water column, but did not report on individual mode excitation. At the same time Ingenito [6] reported on experimental results in shallow water where mode separation was achieved using a weighted vertical receive array. In 1978 Gazanhes *et al.* [8] reported on the identification of individual modes using a weighted receive array in an acoustic tank.

References [9] and [10] conducted mode excitation experiments in acoustic tanks. Clay and Huang [9] conducted experiments at 220 kHz and demonstrated excitation and propagation of the first mode. Gazanhes and Garnier [10] working at 124 kHz used a vertical source array containing 15 sources, whose gain and polarity depended on the mode to be excited, to demonstrate the individual excitation and propagation of modes 1 through 5. It appears that after 1981 there was no further work conducted on the excitation of individual modes in shallow water.

In this section, in order to simplify the discussion, it is assumed that the ocean waveguide is horizontally stratified, i.e., the sound speed varies only with depth. In the subsequent sections this assumption is eliminated. It is well established that under the stratified assumption the solution of the wave equation and boundary conditions

can be expressed as a sum of normal modes. Assuming azimuthal symmetry and using cylindrical coordinates the horizontal distance from the origin to some point in the channel is $r$, and the depth with respect to the ocean surface is $z$ with the depth axis pointing downward. For a harmonic point source at the origin at depth $z_o$ the pressure field in the far field at the point $r, z$ can be expressed as

$$p(r, z; z_o) = \sum_{m=1}^{\infty} \phi_m(z)\phi_m(z_o)H_o^{(1)}(\kappa_m r), \tag{1}$$

where the mode eigenfunctions $\{\phi_m\}$ and the mode eigenvalues $\{\kappa_m\}$ satisfy the equation

$$\frac{\mathrm{d}^2\phi_m(z)}{\mathrm{d}z^2} + \left[\left(\frac{\omega}{c(z)}\right)^2 - \kappa_m^2\right]\phi_m(z) = 0 \tag{2}$$

together with boundary conditions; $H_o^{(1)}$ is the zeroth-order Hankel function of the first kind. The normal mode eigenfunctions $\{\phi_m\}$ form a complete orthonormal set satisfying the orthonormality relation

$$\int_0^{\infty} \rho(z)\phi_n(z)\phi_m(z)\,\mathrm{d}z = \delta_{n,m}, \tag{3}$$

where the density $\rho(z)$ takes an appropriate value in each layer and $\delta_{n,m}$ is the Kronecker delta function.

The mode orthonormality condition of Eq. (3) provides the basis for single-mode excitation. Assume there is a vertical array of sources at the origin located at depths $z_1, z_2, \ldots, z_L$. Furthermore assume that only a finite number of modes $M$ propagate to the point $r, z$ in the field. In this case by applying Eq. (1) the pressure field at the point $r, z$ due to the array of sources is written as

$$p(r, z; z_1, z_2, \ldots, z_L) = \sum_{j=1}^{L} a_j \sum_{m=1}^{M} \phi_m(z_j)\phi_m(z)H_o^{(1)}(\kappa_m r), \tag{4}$$

where the set of coefficients $\{a_j\}$ $j = 1, 2, \ldots, L$ are the shading or weighting coefficients for each of the $L$ sources in the array. Let the weighting coefficients be defined by the eigenfunction of the $n$th mode sampled at the source depths, that is

$$a_j \equiv \phi_n(z_j), \quad j = 1, 2, \ldots, L. \tag{5}$$

In this case the pressure field at the point $r, z$ due to the weighted source array is given by

$$p(r, z; z_1, z_2, \ldots, z_L) = \phi_n(z)H_o^{(1)}(\kappa_n r)\sum_{j=1}^{L} \phi_n^2(z_j) + \sum_{\substack{m=1 \\ m\neq n}}^{M} \gamma_{mn}\phi_m(z)H_o^{(1)}(\kappa_m r), \tag{6}$$

where $\gamma_{mn} \equiv \sum_{j=1}^{L} \phi_m(z_j)\phi_n(z_j)$; note that $\gamma_{mn}$ is a discrete approximation of the integral of Eq. (3). The first term of Eq. (6) represents the field contribution at the point $r, z$ due to mode $n$, the second term represents the cross-mode contributions. By the mode orthonormality condition of Eq. (3) it would be expected that the cross-mode contributions would be small. The magnitude of these contributions are governed by two factors: (1) the spatial sampling scheme used in the source array, and (2) that the discrete approximation is carried out over the depth range of 0 to $z_L$ rather than the full range of 0 to $\infty$.

*B. Optimum frequency* The existence of an optimal frequency band for propagation in shallow water has been known for many years. Early mention of an optimal frequency in shallow water was made by Weston [1] based on measurements taken in the central North Sea over a sand bottom. Those transmission loss measurements showed a substantial dependence on frequency with a frequency of least loss at about 200 Hz. Further work in the Bristol Channel showed an optimal propagation band between 200 and 500 Hz [2]. Jensen and Kuperman [12], comparing theory with experimental results, reported that the optimum frequency of propagation in shallow water is the result of competing propagation and attenuation mechanisms at high and low frequency. Based on measurements made in the North Atlantic they observed an optimum frequency of propagation at around 200 Hz. Eller and Gershfeld investigated the optimum frequency of propagation issue analytically using two canonical bottom models [13]. One model used a fast sediment whose speed was substantially greater than that of water. In this case the acoustic energy was returned from the bottom primarily by reflection at the water/sediment interface. At low frequencies modal attenuation increases with decreasing frequency. That effect was balanced by increasing losses from seawater absorption at higher frequencies, the two effects create a frequency of minimum attenuation. For the second model the sound speed in the sediment had a positive gradient and the speed at the interface was equal to that of the water. In that case the acoustic energy was returned by upward refraction within the sediment. That model also predicted a frequency of least loss, formed by competing effects of seawater absorption at high frequency and bottom interaction at the lower frequencies. In a companion paper the effect of geometric considerations on the optimum frequency of propagation were investigated [18].

*C. Backscattering* The nature of backscatter in shallow water is easily understood in terms of ray theory. At each surface and bottom reflection, new rays are scattered in all directions and a certain number will travel back to the source. It is well established that the use of normal modes for shallow water propagation is advantageous. Thus it is instructive to develop some intuition about the relationship between normal modes and backscatter. Bucker and Morris [19] established a simple theory using a Lambert law–type of scattering function to relate normal modes to the generation of backscatter.

Using the theory of Ref. [19] the total backscatter can be expressed as a double sum over the modes. Let $M$ be the number of modes, ignoring the time-dependent

contributions, we have

$$B = 2\pi\sigma \sum_{m=1}^{M} \sum_{n=1}^{M} |a_m|^2 |a_n|^2 \sin\theta_n \sin\theta_m, \tag{7}$$

where $\sigma$ is a scattering coefficient, $a_m$ is the mode amplitude for the $m$th mode and $\theta_m$ is the grazing angle for the $m$th mode. Using Eq. (7) we can define a mode scattering term for each mode,

$$B_n = 2\pi\sigma |a_n|^2 \sin\theta_n \sum_{m=1}^{M} |a_m|^2 \sin\theta_m. \tag{8}$$

For any mode $n$ the sum over the modes, $\sum_{m=1}^{M} |a_m|^2 \sin\theta_m$, is a constant. Thus dropping the constant terms we can approximate the mode scattering terms by

$$B_n = |a_n|^2 \sin\theta_n \tag{9}$$

for each mode $n = 1, 2, \ldots, M$. It is obvious that the scattering is strongly dependent on the mode grazing angle.

Consider a simple example, a Pekeris channel with water depth 100 m, sound speed 1500 m/s, bottom sound speed 1800 m/s, density 2 g/cm$^3$, and bottom attenuation 0.7 dB/$\lambda$. For this channel, at a frequency of 200 Hz, a source at 50 m and at a range of 4900 m from the source the distribution of relative mode amplitudes is presented in Fig. 1.

From Fig. 1 it is seen that the odd-numbered modes, up to mode 13, have relatively large mode amplitudes. For this channel the grazing angle is 2° for mode 1 and increases almost linearly with mode number up to 44° for mode 20. Using Eq. (9) it is easy to approximate the scattering contribution for each of the modes; this result is contained in Table 1.

These seven dominant modes represent approximately 75% of the total backscatter as seen by summing over the last column of Table 1. Even though the mode 1 amplitude is the largest, since its grazing angle is the smallest, the mode 1 contribution ($B_1 = 0.03$) is seen to be the smallest. Furthermore it is apparent that the mode 1 contribution is only a very small part of the total backscatter. This type of simple relative scattering calculation clearly illustrates the advantage of single mode excitation for backscatter reduction. In order to analyze the backscatter for realistic situations a numerical backscatter model was employed [14].

It is well known that the parabolic equation (PE) method is efficient for solving acoustic propagation problems with range-dependent environments. Recently the PE method was extended to handle backscatter from deterministic deformations in the boundaries, this version is referred to as the two-way PE [14]. The two-way PE is based on a single-scattering approximation and the approach of two-way coupled

**Table 1** *Relative backscatter as a function of mode number for the Pekeris channel*

| Mode number | $\theta$ (deg) | $\lvert a\rvert^2$ | $\sin\theta$ | $B_n$ |
|---|---|---|---|---|
| 1 | 2.0 | 1.00 | 0.03 | 0.03 |
| 3 | 6.2 | 0.90 | 0.10 | 0.09 |
| 5 | 10.3 | 0.72 | 0.18 | 0.13 |
| 7 | 14.6 | 0.56 | 0.25 | 0.14 |
| 9 | 19.0 | 0.42 | 0.32 | 0.14 |
| 11 | 23.5 | 0.30 | 0.40 | 0.12 |
| 13 | 28.2 | 0.20 | 0.47 | 0.09 |

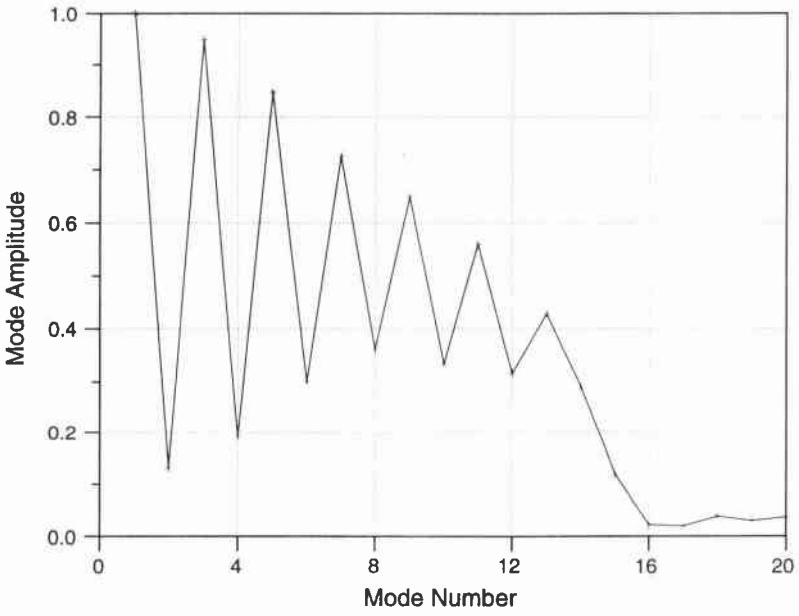


**Figure 1** *Relative mode amplitudes for the Pekeris channel at 200 Hz.*

modes in which range-dependent environments are approximated by a sequence of range-independent regions. At the vertical boundaries between regions the solution of the two-way PE is required to satisfy continuity conditions. Note, as discussed in Ref. [14], in order to avoid the unrealistic focusing and multiple scattering that occurs for a point source in cylindrical geometry the two-way PE was implemented as a line source in plane geometry, the spreading factor $r^{-1/2}$ is not included in the field computation.

As with all PE based propagation codes the forward propagation was initiated with a 'starting-field'. For this application a mode-based starting-field which was a function of the source depth was used. This application required a vertical array of sources

to be used rather than a single omni-directional source, thus the PE starting-field was modified to incorporate multiple sources as follows. Let $\boldsymbol{w}_j(z)$ be the starting-field pressure vector for a source at depth $z_j$, i.e., pressure vs depth sampled on some grid as generated by the mode-based field starter. Then by Eq. (4) it follows that the total starting-field vector $\boldsymbol{u}(z)$ for a source array with sources at depths $z_1, z_2, \ldots, z_L$ is given by

$$\boldsymbol{u}(z) = a_1\boldsymbol{w}_1(z) + a_2\boldsymbol{w}_2(z) + \cdots + a_L\boldsymbol{w}_L(z), \tag{10}$$

where the set $\{a_j\}$, $j = 1, 2, \ldots, L$, are weighting coefficients used to effect single-mode excitation. To facilitate comparing backscattered fields for various source array configurations, the weighting coefficients were normalized for constant power, i.e., $\sum_{j=1}^{L} a_j^2 = 1$.

Given the starting-field $\boldsymbol{u}(z)$ the PE solution proceeds in two steps. Starting at the source array, $r = 0$, the outgoing PE is used to propagate the forward field across the range-independent regions. In regions in which backscattering is expected to be important, transmitted (forward-scattered) and reflected (backscattered) fields are computed at the vertical interfaces between range-independent regions. The reflected fields are stored for later use. After this process has reached the maximum range, the incoming PE is used to propagate the incoming reflected fields. See Ref. [14] for further details on the PE-based scattering method.

# 3

# Shallow-water acoustic response

Since both attenuation and backscatter are affected by the geoacoustic parameters of the sediment, the analysis was carried using three different canonical geoacoustic models. All models contained a homogeneous sediment layer 450 m thick with a highly attenuating infinite half-space below the sediment, $\alpha_c = 10$ dB/$\lambda$. The first model, model A (coarse sand), represented a situation where the compressional speed in the sediment was high the density was high and the acoustic energy was returned primarily by reflection at the water/sediment interface. Model B (silt) represented a 'softer' sediment situation. Both the compressional speed and density were closer to the water values at the interface. Model C (clayey silt) represented a situation where the sediment density was lower than models A and B and the compressional speed was close to the water value at the interface. These three models represent a wide variation of sediment types. The sediment parameters are from Ref. [13]. Table 2 summarizes the geoacoustic parameters for the three canonical models.

The plane-wave reflection loss at the water/sediment interface as a function of grazing angle was evaluated for each of the canonical geoacoustic models, using the relationships from Ref. [13]. The magnitude of the plane-wave reflection coefficient was evaluated for each of the three canonical models over a range of grazing angles from 0° to 35°. The results are illustrated by Fig. 2 and an estimate of the critical angle is included in Table 2.

As expected for model A with the coarse sand sediment the critical angle is quite large, on the order of 32°, and the reflection loss coefficient is small. Models B and C represent intermediate cases with critical angles of around 17° and 7°, respectively. As indicated by Fig. 2 the range of critical angles and bottom reflection loss coefficients is fairly large, thus these three canonical geoacoustic models represent a wide variety of propagation conditions.

For evaluation of attenuation with range vs frequency both a winter and summer sound-speed profile was included, see Fig. 3.

The attenuation coefficient associated with the first mode for each of the canonical models was evaluated as a function of frequency using the SACLANTCEN normal mode model, SNAP [20]. These results are illustrated in Fig. 4.

Figure 4a illustrates the attenuation of mode 1 for the three canonical models using the winter profile. The results are quite interesting. Note the strong dependence on frequency for all models. For each model the transition frequency where sediment

**Table 2** *Geoacoustic parameters for the three canonical models*

| Model | Sediment type | Relative density $\rho_s/\rho_w$ | Relative speed $c_s/c_w$ | Compressional speed $c_s$ (m/s) | Compressional attenuation $\alpha$ (dB/$\lambda$) | Critical angle $\theta_c$ (deg) |
|---|---|---|---|---|---|---|
| A | coarse sand | 2.03 | 1.20 | 1800 | 0.70 | 32 |
| B | silt | 1.77 | 1.06 | 1593 | 1.02 | 17 |
| C | clayey silt | 1.47 | 1.01 | 1516 | 0.12 | 7 |

attenuation is a minimum and the seawater absorption is a minimum is clearly indicated. For model A the minimum is in the 200 to 300 Hz region, while for models B and C the minimum has moved up in frequency to about 250 to 500 Hz. Fig. 4b illustrates the situation using the summer sound-speed profile. Overall the attenuation is higher for the summer case and the minimum as a function of frequency is not as pronounced as it was for the winter case. For the summer case the minimum for model A occurs at about the same frequency as for the winter case. But for models B and C the minimum has moved up in frequency to about 600 Hz. From the results of Figures 4a and 4b, it is clear that a frequency band of minimum attenuation can be selected for the propagation of mode 1 for each of the geoacoustic models.

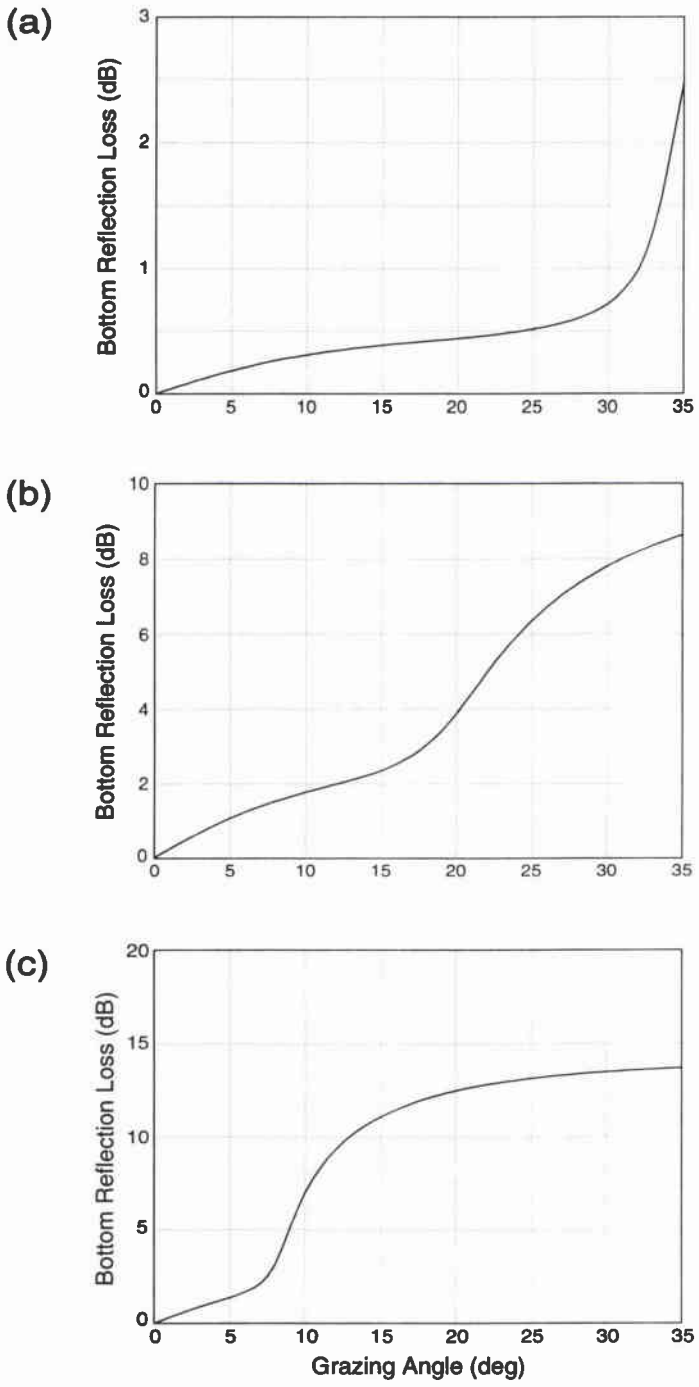


**Figure 2** *Bottom reflection loss at the water/sediment interface: (a) model A – coarse sand, (b) model B – silt, (c) model C – clayey silt.*

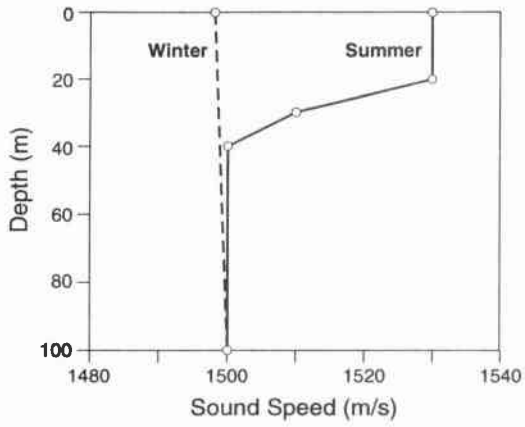


**Figure 3** *The canonical sound-speed profiles for winter and summer.*

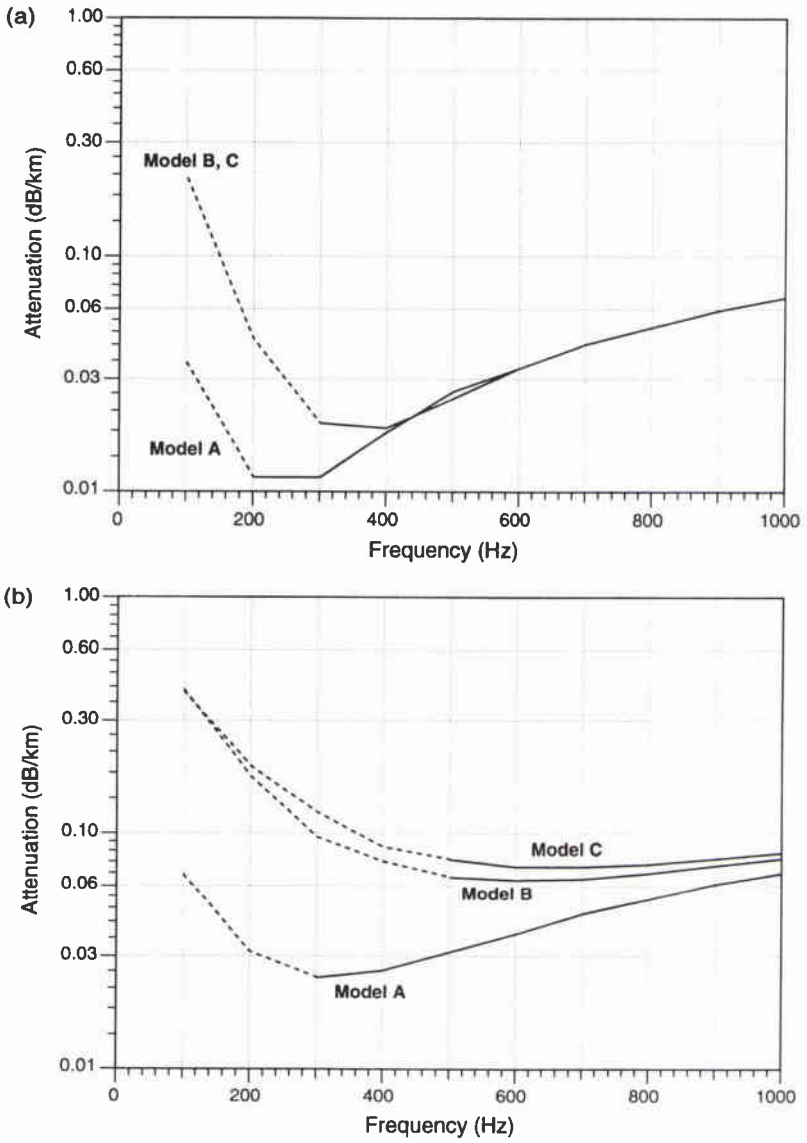


**Figure 4** *Mode 1 attenuation as a function of frequency: (a) winter and (b) summer. The dashed portion indicates the frequency region where the sediment attenuation is greater than that due to seawater absorption.*

# 4

# Backscatter simulation results

In this section the results obtained using the two-way PE method to evaluate backscatter as a function of frequency are presented. Results are presented for the three canonical geoacoustic models using both the winter and summer sound-speed profiles. The effect of shear was not included in the backscatter simulations. The backscatter results presented are the result of averaging over backscatter calculations computed using multiple realizations of random bathymetry profiles.

*A. Bathymetry model* The bathymetry profile or two-dimensional surface height function, $h_n$ where the index $n$ represents the range variable, is treated as a discrete random process. That is, for any value of $n$, $h_n$ is a random variable whose properties are determined by some underlying probability distribution function. The numerical generation of the surface height function usually involves the application of linear stochastic models. The correct choice of the linear model parameters allows for careful control of the statistics of the surface realizations, such as height probability distribution and autocorrelation function properties [21].

The random variable $h_n$ represents the surface height at some range $r_n = n\Delta r$, where $\Delta r$ represents the discretization interval on the range axis. Linear models such as autoregressive (AR) and moving average (MA) are often used, see [22]. For the analysis presented herein an autoregressive process model was used. In this case the surface height random process is defined by

$$h_n = \sum_{l=1}^{N} \phi_l h_{n-l} + u_n, \tag{11}$$

where $u_n$ is an uncorrelated random process with variance $\sigma_u^2$, $N$ is the order of the process, and the set of coefficients $\{\phi_l\}$ are the constants which control the statistical properties. A first-order autoregressive process AR(1) was used, which for this case gives

$$h_n = \phi h_{n-1} + u_n. \tag{12}$$

Under the assumption that $|\phi| < 1$ the process is considered to be asymptotically stationary (up to order 2) with the surface autocorrelation function given by

$$C_n = \phi^{|n|} \tag{13}$$

which, for $\phi > 0$, is an exponentially decaying function.

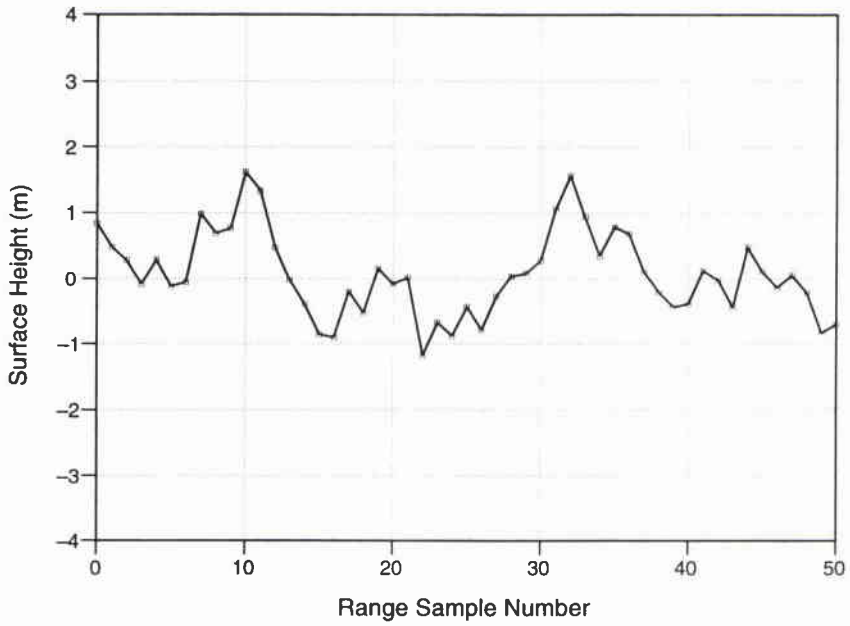


**Figure 5** *Single realization of AR(1) random surface height generated with* $\sigma_u^2 = 0.25$ *m and* $\phi = 0.8$.

For the analysis conducted herein large-scale slow variations of bathymetry as a function of range were desired. Thus, the surface realizations were generated using a highly correlated first-order autoregressive process driven by an uncorrelated Gaussian process with variance $\sigma_u^2 = 0.25$ m. The AR coefficient $\phi$ was set equal to 0.8 which provides a high degree of correlation. From Eq. (13) the autocorrelation is seen to be on the order of 0.5 at $n = 3$ for the above-described AR(1) process. The variance of the surface height process is given by

$$\sigma_h^2 = \frac{\sigma_u^2}{(1-\phi^2)}. \tag{14}$$

By Eq. (14) with the variance of the Gaussian process $u_n$ set at 0.25 m and the AR coefficient $\phi$ set to 0.8, the resulting standard-deviation for the surface height process $h_n$ was 0.83 m. Figure 5 illustrates an example realization of a random surface height function generated using the AR(1) model.

Examining Fig. 5 it is seen that this AR(1) model, with $\Delta r = 100$ m, provides the type of large-scale slowly varying bathymetry vs range profile that was desired, that is on the order of $\pm 1$ m of surface height variation over 1 km.

For each realization of the surface height random process a realization of a bathymetry vs range profile was constructed for input to the two-way PE propagation model. The bathymetry vs range profile contained a deterministic component, constant as a function of range, and a zero-mean Gaussian component generated by the

random surface height function, see Eq. (12). For each realization of a bathymetry profile the forward and backscattered field was computed. The final forward and backscattered fields were the result of averaging the fields over multiple realizations to minimize the effect of statistical fluctuations.

*B. Average backscatter* The objective of the Monte Carlo simulations was to evaluate bottom-generated backscatter as a function of frequency, season, and sediment properties. The average backscatter as a function of frequency was computed for each of the three geoacoustic models, see Table 1, using the winter and summer sound-speed profiles of Fig. 3. In all cases the backscattered field was computed over the range interval from 0 to 5 km for 20 realizations of random bathymetry profiles. The average backscatter was formed by averaging over the 20 realizations and then calculating an average for the field from 0 to 5 km at one depth. The bathymetry vs range realizations were calculated using a range step interval of 100 m. The deterministic component of the bathymetry was set to 100 m.

Figure 6 illustrates the average backscatter as a function of frequency for a single source at 50 m for the winter profile. The backscatter at three receiver depths, 40, 50 and 60 m, is presented for the three geoacoustic models. There is almost no variation of the average backscatter as a function of receiver depth. For this case, a single source at 50 m, it is seen that there is only a fairly small variation of the average backscatter as a function of frequency, the backscatter increasing with increasing frequency. The dependence of the average backscatter on geoacoustic parameters is seen to be significant. For model A, the highly reflecting case (largest critical angle), the average backscatter is the largest of the three models. There is a substantial difference, 15 dB, for the average backscatter between that obtained with model A vs model C. This large difference follows directly from the difference in transmission loss for the three models.

Figure 6 illustrates the average backscatter as a function of frequency for a single source at 50 m for the summer profile. Overall the backscatter versus frequency as a function of geoacoustic model are about the same for the winter and summer profiles.

Table 3 illustrates the source array configurations used for the winter profile. The source-to-source spacing varied with frequency to account for the fact that the shape of the mode 1 eigenfunction varies with frequency and season, see Fig. 8.

For example, at 200 Hz the winter mode 1 eigenfunction is non-zero over the entire water column, but at 1000 Hz the eigenfunction is only non-zero over the interval from 0 to 60 m. Thus the source-to-source spacing was adjusted with frequency in an attempt to keep most of the sources in the non-zero portion of the eigenfunction. The selection of the array source positions in the water column could be optimized to provide a configuration that is 'optimum' with respect to backscatter reduction. This optimization could not feasibly be carried out over all frequencies and all geoacoustic models, thus the configurations of Table 3 may not provide the best results

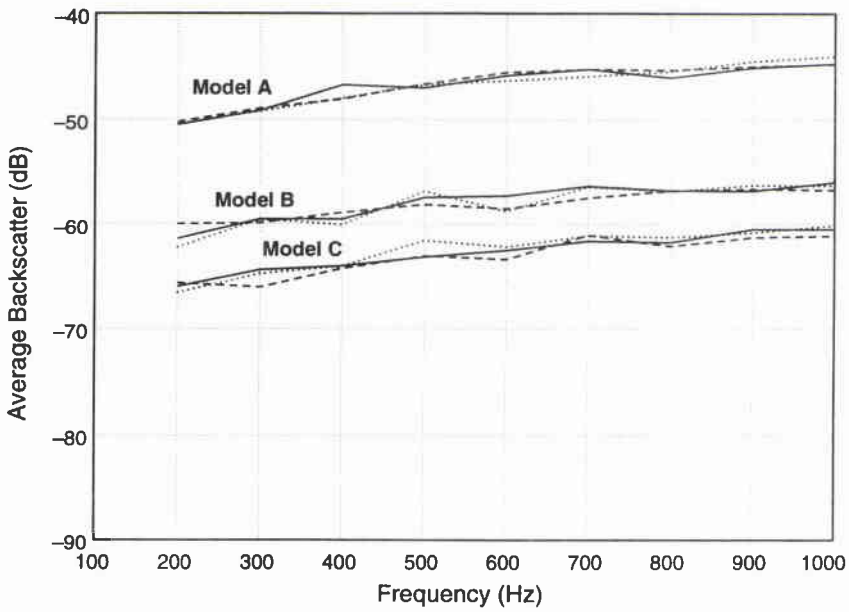


**Figure 6** *Average backscatter as a function of frequency for one source at 50 m at three receiver depths, 40 m (dotted), 50 m (solid), and 60 m (dashed), for the winter profile.*

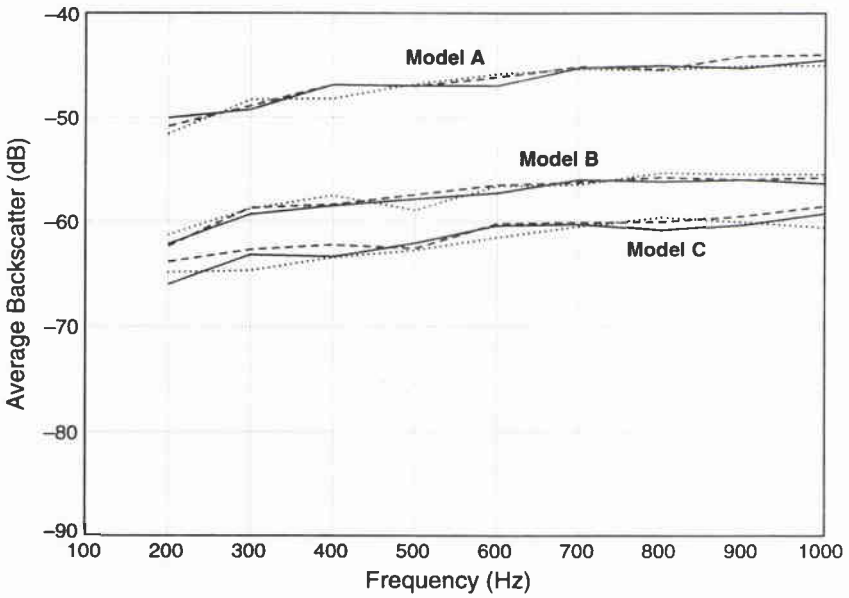


**Figure 7** *Average backscatter as a function of frequency for one source at 50 m at three receiver depths, 40 m (dotted), 50 m (solid), and 60 m (dashed), for the summer profile.*

**Table 3** *Source array configurations as a function of frequency for the winter profile*

| Freq. (Hz) | 12 Sources | | | 24 Sources | | |
|---|---|---|---|---|---|---|
| | first source (m) | last source (m) | source spacing (m) | first source (m) | last source (m) | source spacing (m) |
| 200 | 2.0 | 94.4 | 8.4 | 2.0 | 98.6 | 4.2 |
| 300 | 2.0 | 94.4 | 8.4 | 2.0 | 98.6 | 4.2 |
| 400 | 2.0 | 94.4 | 8.4 | 2.0 | 98.6 | 4.2 |
| 500 | 2.0 | 90.0 | 8.0 | 2.0 | 94.0 | 4.0 |
| 600 | 2.0 | 90.0 | 8.0 | 2.0 | 94.0 | 4.0 |
| 700 | 2.0 | 76.8 | 6.8 | 2.0 | 80.2 | 3.4 |
| 800 | 2.0 | 72.4 | 6.4 | 2.0 | 75.6 | 3.2 |
| 900 | 2.0 | 68.0 | 6.0 | 2.0 | 71.0 | 3.0 |
| 1000 | 2.0 | 63.6 | 5.6 | 2.0 | 66.4 | 2.8 |

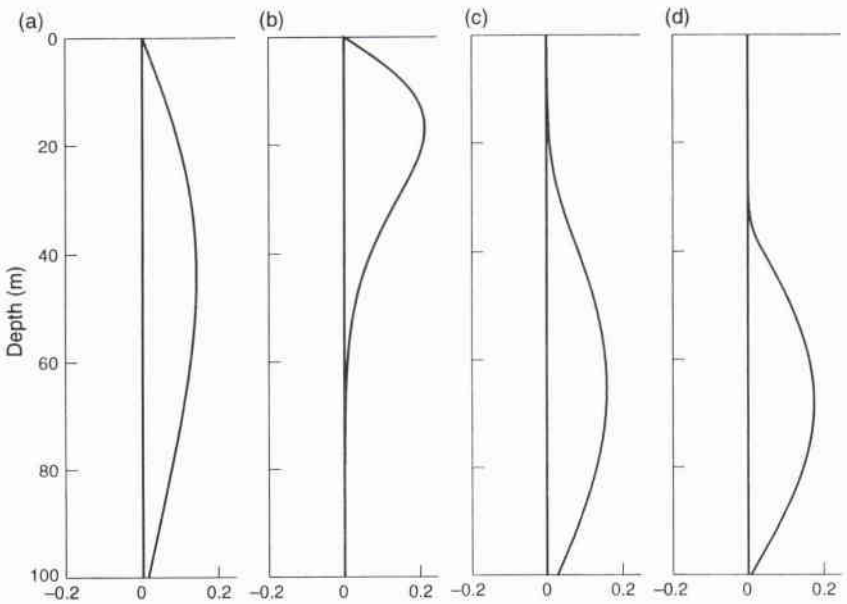


**Figure 8** *Mode one eigenfunction as a function of depth, model A: (a) winter, 200 Hz; (b) winter, 1000 Hz; (c) summer, 200 Hz; and (d) summer, 1000 Hz.*

(minimum backscatter) obtainable. These configurations do provide a good indication of the performance that could be expected. Some of the variability of the average backscatter as a function of frequency observed in the results presented below may be due to a non-optimum array configuration at a particular frequency. Table 4 provides the source array configurations used for summer profile.

Figure 9 illustrates average backscatter for geoacoustic model A with the winter profile. The average backscatter was calculated for three source array configurations

**Table 4** *Source array configurations as a function of frequency for the summer profile*

| Freq. (Hz) | 12 Sources | | | 24 Sources | | |
|---|---|---|---|---|---|---|
| | first source (m) | last source (m) | source spacing (m) | first source (m) | last source (m) | source spacing (m) |
| 200 | 18.0 | 97.2 | 7.2 | 15.0 | 97.8 | 3.6 |
| 300 | 23.0 | 97.8 | 6.8 | 20.0 | 98.2 | 3.4 |
| 400 | 27.0 | 97.4 | 6.4 | 25.0 | 98.6 | 3.2 |
| 500 | 30.0 | 96.0 | 6.0 | 28.0 | 97.0 | 3.0 |
| 600 | 33.0 | 96.8 | 5.8 | 31.0 | 97.7 | 2.9 |
| 700 | 33.0 | 96.8 | 5.8 | 31.0 | 97.7 | 2.9 |
| 800 | 35.0 | 96.6 | 5.6 | 33.0 | 97.4 | 2.8 |
| 900 | 35.0 | 96.6 | 5.6 | 33.0 | 97.4 | 2.8 |
| 1000 | 35.0 | 96.6 | 5.6 | 33.0 | 97.4 | 2.8 |

(one source at 50 m, 12 sources, and 24 sources as in Table 3) as a function of frequency. As shown by Fig. 6 there was little variation of the backscatter as a function of frequency when there was only one source. The average backscatter for the source array with 12 sources was substantially below that for a single source in the lower part the frequency band, that is below 400 Hz. Above 400 Hz there was no advantage (less backscatter than single source) when the source array with 12 sources was used. The reduction at 200 Hz was on the order of 12 dB. At the higher frequencies, above 400 Hz, 12 sources were not sufficient to eliminate the higher-order mode excitation and thus were not as effective at reducing the backscatter. Alternatively, for the source array with 24 sources, there was a substantial reduction of the bottom-generated backscatter across the entire frequency band. The reduction was most significant, 18 to 24 dB with respect to the single-source case, in the band from 300 to 450 Hz. Overall, for geoacoustic model A, the use of a source array with 24 sources weighted to excite mode 1 significantly reduced the bottom-generated backscatter over the band from 200 to 1000 Hz with the band from 300 to 450 providing the minimum backscatter.

Figure 10 illustrates average backscatter for geoacoustic model A as a function of frequency with the summer profile. The summer results were quite similar to those obtained using the winter profile except that there was not a null in backscatter in the 300 to 450 Hz band. For the summer profile the backscatter reduction due to using source arrays with 24 sources was fairly uniform as a function of frequency across the band from 300 to 700 Hz. The average reduction was on the order of 12 dB across the band. As with the winter profile a source array with 24 sources was required to obtain significant reduction of backscatter over a large band. For the summer profile an anomaly is noted at 200 Hz, the average backscatter is greater for the 24 source array than for the 12 source array, whereas for the winter profile the backscatter was the same for both source arrays. Examining the mode 1 eigenfunctions for 200 Hz, see Fig. 8, it can be seen that the value of the summer mode 1 eigenfunction at the water/sediment interface is greater than that for the winter profile. The result

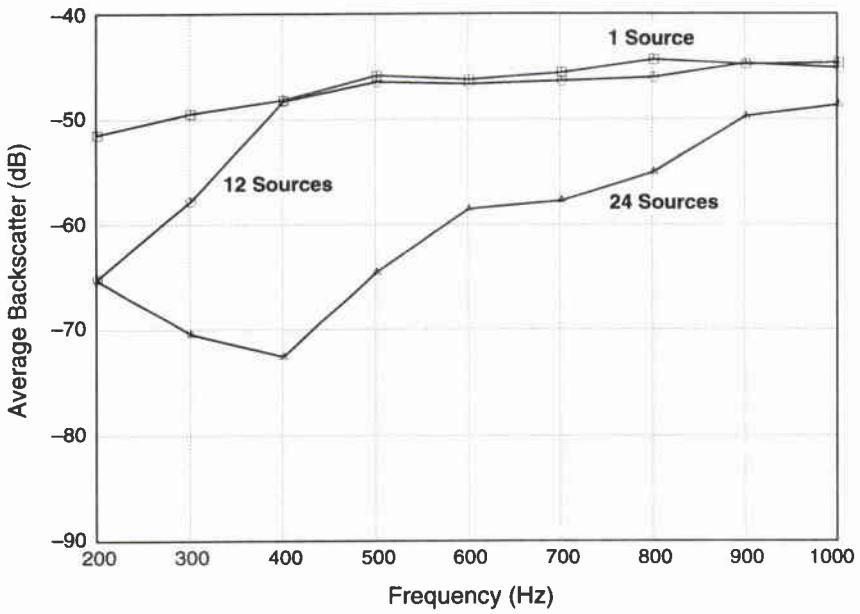


**Figure 9** *Average backscatter at 50 m as a function of frequency for model A using three source arrays, winter profile.*

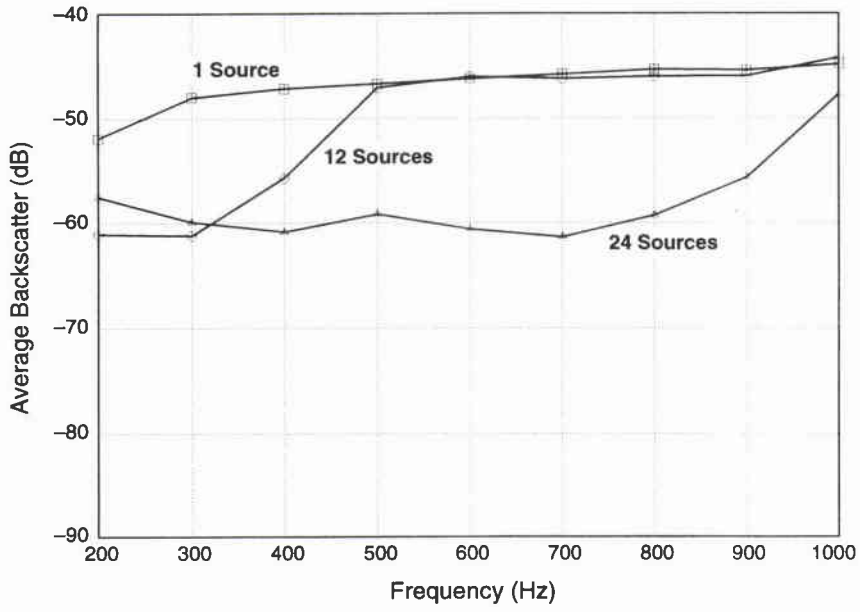


**Figure 10** *Average backscatter at 50 m as a function of frequency for model A using three source arrays, summer profile.*

being that excitation of this mode eigenfunction near the water/sediment interface actually directs more energy onto the bottom and thus more backscatter.

Figure 11 illustrates average backscatter for geoacoustic model B with the winter profile. For this model the average backscatter for all three source array configurations was less than those for model A. The source array with 12 sources provided a reduction, with respect to that obtained with one source, across the entire frequency band varying from 2 to 10 dB. Above 600 Hz the source array with 12 sources did not provide a significant reduction of the backscatter. The source array with 24 sources provided a substantial reduction (about 16 dB) for the average backscatter across the band from 350 to 1000 Hz, with the minimum backscatter level at 400 Hz.

Figure 12 illustrates the average backscatter for model B with the summer profile. It is seen that with the summer profile the effectiveness of the multiple source arrays for backscatter reduction is less than for the winter profile. The reduction is greatest across the band from 700 to 1000 Hz for the 24 source array. For frequencies below 600 Hz the 12 source array is slightly more effective, again because of the shape of the summer mode 1 eigenfunction at the sediment interface.

Figure 13 illustrates the average backscatter for geoacoustic model C with the winter profile. For this geoacoustic model the average backscatter for all three source array configurations is less than that for models A and B. The source array with 12 sources provided a reduction, with respect to that obtained with one source, of 13 dB in the band from 400 to 800 Hz. The result obtained using 24 sources is on average about 4 dB better than that obtained with 12 sources. The result for the source array with 24 sources is quite impressive, the reduction is on the order of 16 dB across the band from 400 to 1000 Hz.

For geoacoustic model C with the summer profile, the average backscatter results are presented on Fig. 14. For this case the backscatter reduction is only on the order of 2 dB below 400 Hz. Above 400 Hz the reduction varies from 4 dB to 8 dB. The band from 700 to 1000 provides the greatest reduction. Overall the source array with 12 sources outperforms the 24 source array.

For the summer profile case the mode 1 eigenfunction was non-zero at the water/sediment interface at the lower frequencies. The amplitude of this non-zero component at the water/sediment interface was a function of both the geoacoustic model and frequency. For the lower frequencies, where there was a non-zero amplitude, the source array with 24 sources produced more backscatter than the 12-source array because of the non-zero component at the water/sediment interface. For each of the geoacoustic models there was a frequency at which this component went to zero, and thus the 24-source array outperformed the 12-source array. For model A this occurred at 300 Hz, for model B at 600 Hz, and for model C at 900 Hz.

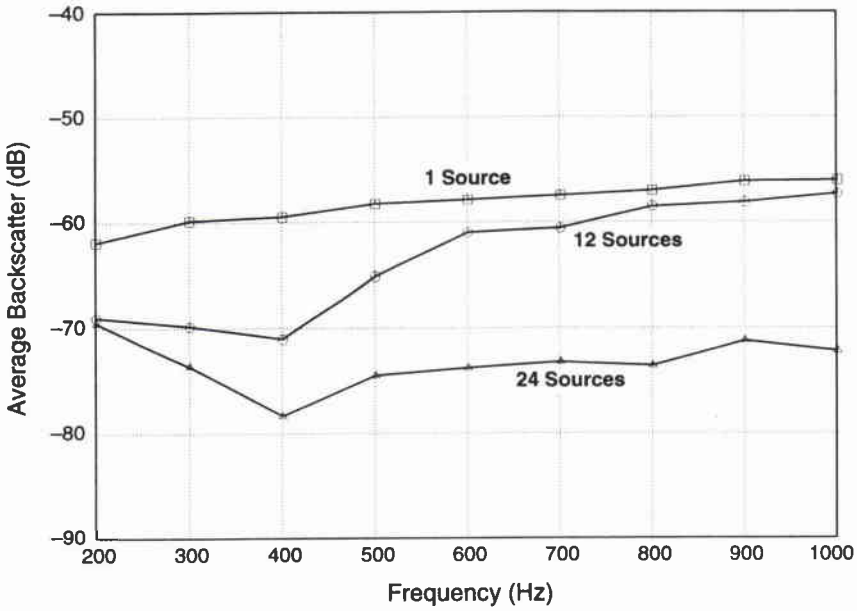


**Figure 11** *Average backscatter at 50 m as a function of frequency for model B using three source arrays, winter profile.*

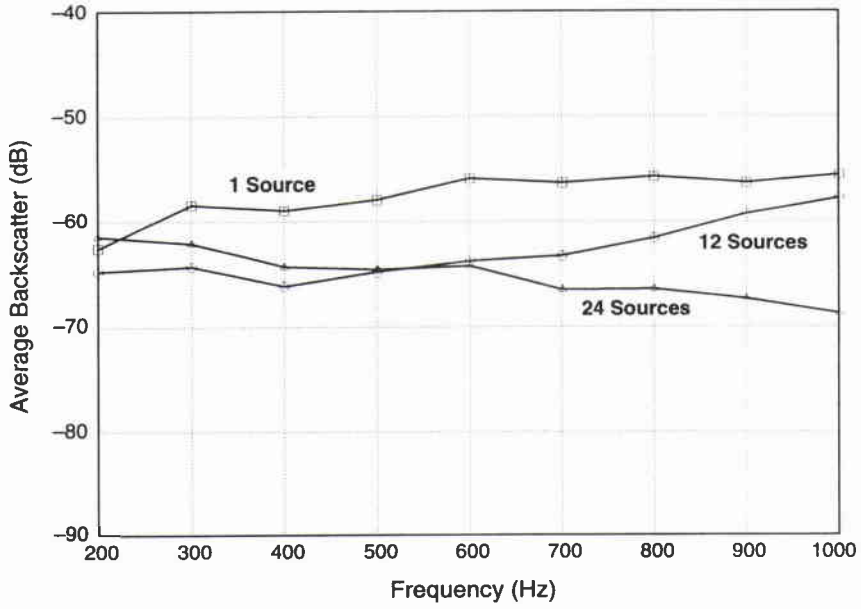


**Figure 12** *Average backscatter at 50 m as a function of frequency for model B using three source arrays, summer profile.*

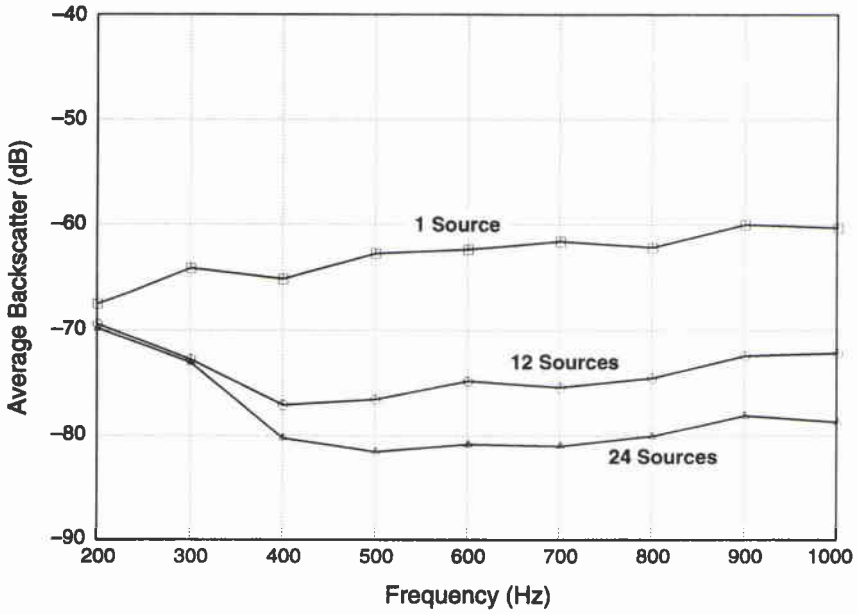


**Figure 13** *Average backscatter at 50 m as a function of frequency for model C using three source arrays, winter profile.*

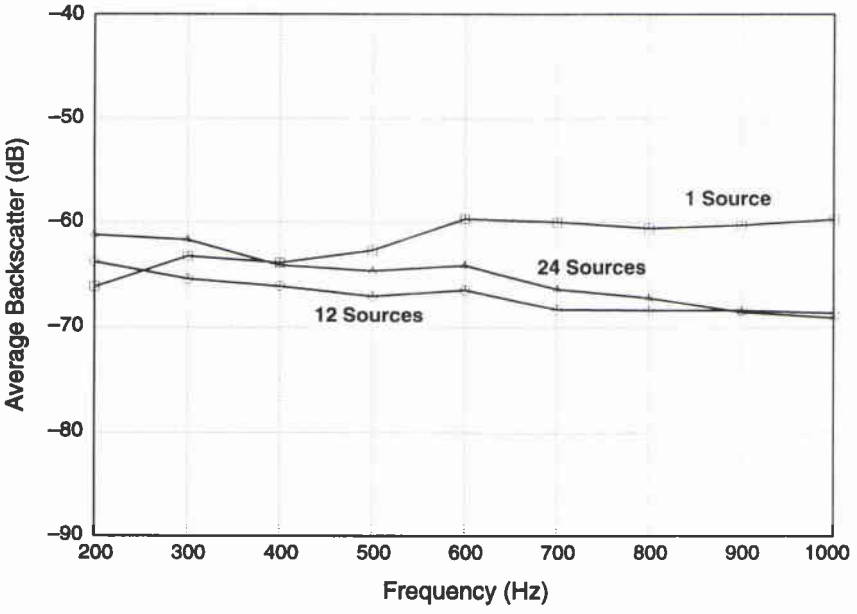


**Figure 14** *Average backscatter at 50 m as a function of frequency for model C using three source arrays, summer profile.*

# 5 Summary

In this section the combined results for minimum attenuation and minimum backscatter are discussed. We first consider the winter profile. Examining Fig. 4a it is apparent that there is a well-defined minimum for attenuation as a function of frequency for each of the geoacoustic models. Comparing Figs. 9, 11 and 13, a frequency band of minimum backscatter can also be identified. Overall, the backscatter reduction obtained using a source array with 24 sources was significant over a large band for all three geoacoustic models. A band of both minimum attenuation and backscatter can be identified. These results are compiled in Table 5.

The last column of Table 5 contains the limits for the frequency band of minimum attenuation and minimum backscatter for the winter profile. For this profile the (width of the) optimum band for both minimum attenuation and backscatter is fairly narrow, i.e., 100 to 150 Hz, because there is only a fairly limited region of overlap for the two bands. The center frequency of the optimum band increases as a function of the geoacoustic model from A to C, clearly indicating that the properties of the sediment are an important factor in the selection of an operating band. Note also that the amount of backscatter reduction is also dependent on the sediment properties.

Similar results were compiled using Figs. 4b, 10, 12 and 14 for the summer profile, see Table 6. For this case, since the mode 1 attenuation is fairly flat as a function of frequency, it is seen that the optimum bands are wider, i.e., 300 Hz. Overall for the summer profile the backscatter reduction is less than that obtained for the winter profile.

From Figs. 6 and 7 it was seen that the seasonal (winter vs summer) effect was small when one source was used. But when mode 1 excitation was used the seasonal effect was seen to be important. This of course follows directly from the shape of the mode 1 eigenfunctions. The mode 1 eigenfunction for the summer profile 'peaks' closer to the water/sediment interface than that for the winter profile, see Fig. 8. It should be noted, even though the backscatter reduction for the summer profile is not as significant as that for the winter profile there remains a significant reduction for all three models with respect to a single source.

In summary, it appears that the use of source arrays with multiple sources weighted in amplitude and polarity to excite the mode 1 eigenfunction provides a significant improvement in terms of minimizing both attenuation and backscatter for a wide variety of geoacoustic models and for a wide range of frequencies. While the sim-

**Table 5** *Frequency bands of minimum attenuation and backscatter for the winter sound-speed profile*

| Geoacoustic model | Minimum attenuation band (Hz) | Minimum backscatter band (Hz) | Maximum backscatter reduction (dB) | Combined best band (Hz) |
|---|---|---|---|---|
| A | 150–400 | 300–450 | 24 | 300–400 |
| B | 250–500 | 350–800 | 18 | 350–500 |
| C | 250–500 | 400–800 | 18 | 400–500 |

**Table 6** *Frequency bands of minimum attenuation and backscatter for the summer sound-speed profile*

| Geoacoustic model | Minimum attenuation band (Hz) | Minimum backscatter band (Hz) | Maximum backscatter reduction (dB) | Combined best band (Hz) |
|---|---|---|---|---|
| A | 200–600 | 300–700 | 16 | 300–600 |
| B | 400–1000 | 700–1000 | 12 | 700–1000 |
| C | 400–1000 | 700–1000 | 8 | 700–1000 |

ulations were limited to the 200 to 1000 Hz band the results of the backscatter computations indicate that backscatter reduction via mode 1 excitation may well be effective at frequencies above 1000 Hz.

Report no.changed (Mar 2006): SR-236-UU

# Document Data Sheet

| Security Classification | | Project No. |
|---|---|---|
| | | 02 |
| **Document Serial No.** | **Date of Issue** | **Total Pages** |
| SR-236 | October 1995 | 33 pp. |

*Author(s)*

D.F. Gingras

*Title*

Single mode excitation, attenuation and backscatter in shallow water

*Abstract*

Normal mode theory is used to illustrate that a vertical array of weighted sources driven in an appropriate frequency band can be used to minimize the combined effects of attenuation and bottom-generated backscatter in shallow water. Results are presented for three canonical geoacoustic models using both a winter and summer sound speed profile. It is shown that through selective excitation of only mode 1 there exists an optimum frequency band providing both minimum attenuation and minimum bottom-generated backscatter. The results indicate that the center frequency of the optimum band increases as the critical angle decreases.

*Keywords*

attenuation, bottom backscatter, geoacoustic models, selective excitation, shallow water

*Issuing Organization*

North Atlantic Treaty Organization
SACLANT Undersea Research Centre
Viale San Bartolomeo 400, 19138 La Spezia, Italy

*[From N. America: SACLANTCEN CMR-426 (New York) APO AE 09613]*

tel: +39-187-540.111
fax: +39-187-524.600

e-mail: library@saclantc.nato.int

## Initial Distribution for SR-236

| | |
|---|---|
| *Ministries of Defence* | |
| DND Canada | 10 |
| CHOD Denmark | 8 |
| DGA France | 8 |
| MOD Germany | 15 |
| HNDGS Greece | 11 |
| MARISTAT Italy | 10 |
| MOD (Navy) Netherlands | 12 |
| NDRE Norway | 10 |
| MDN Portugal | 5 |
| MOD Spain | 2 |
| TDKK Turkey | 5 |
| MOD UK | 20 |
| ONR US | 54 |
| *NATO Authorities* | |
| NAMILCOM | 2 |
| SACLANT | 3 |
| CINCIBERLANT | 1 |
| COMSUBACLANT | 1 |
| *SCNR for SACLANTCEN* | |
| SCNR Belgium | 1 |
| SCNR Canada | 1 |
| SCNR Denmark | 1 |
| SCNR Germany | 1 |
| SCNR Greece | 1 |
| SCNR Italy | 1 |
| SCNR Netherlands | 1 |
| SCNR Norway | 1 |
| SCNR Portugal | 1 |
| SCNR Spain | 1 |
| SCNR Turkey | 1 |
| SCNR UK | 1 |
| SCNR US | 2 |
| French Delegate | 1 |
| SECGEN Rep. SCNR | 1 |
| NAMILCOM Rep. SCNR | 1 |
| *National Liaison Officers* | |
| NLO Belgium | 1 |
| NLO Canada | 1 |
| NLO Denmark | 1 |
| NLO Germany | 1 |
| NLO Italy | 1 |
| NLO Netherlands | 1 |
| NLO UK | 1 |
| NLO US | 1 |
| Total external distribution | 202 |
| SACLANTCEN Library | 23 |
| Total number of copies | 225 |